Generalizable Deepfake Detection via Artifact-Invariant Representation Learning

Divyanshu Parihar
Independent Researcher
divyanshu1447@gmail.com

Abstract—Deepfake detection has emerged as a critical challenge in digital forensics, yet current detectors consistently fail when encountering generators unseen during training. This phenomenon, known as the "generalization gap," arises from models memorizing dataset-specific compression artifacts rather than learning universal forgery signatures. We propose an Artifact-Invariant Representation Learning (AIRL) framework that addresses this fundamental limitation by focusing on high-frequency spectral residuals—the mathematical fingerprints left behind by generative upsampling operations that persist across different synthesis methods. Our approach employs a dual-stream architecture that fuses semantic RGB features extracted via EfficientNet-B4 with frequency-domain noise maps obtained through Discrete Cosine Transform (DCT) analysis. We further introduce a supervised contrastive learning objective that clusters all synthetic faces together regardless of their generator origin, forcing the network to learn manipulation-agnostic representations. Extensive experiments on cross-domain benchmarks demonstrate that our method achieves 84.7% AUC when training on FaceForensics++ and testing on Celeb-DF, representing a 19.3 percentage point improvement over the widely-used Xception baseline which collapses to 65.4%. Our approach also demonstrates remarkable robustness to post-processing degradations, maintaining 78.8% AUC under combined blur and JPEG compression where competing methods drop below 50%. We provide comprehensive ablation studies validating the contribution of each component and release our implementation to facilitate future research in generalizable deepfake detection.

Index Terms—Artifact invariance, biometrics, deepfake forensics, domain generalization, spectral analysis, contrastive learning, frequency-domain analysis

I. INTRODUCTION

The proliferation of AI-generated synthetic media poses unprecedented challenges to digital trust and information integrity. Deepfake technology, which leverages deep learning to synthesize realistic facial manipulations, has evolved from academic curiosity to a genuine societal threat. From non-consensual intimate imagery to political misinformation campaigns, the malicious applications of this technology continue to expand as generation quality improves and creation tools become democratized.

The forensic community has responded with increasingly sophisticated detection methods, yet a fundamental problem persists: detectors trained on one generation method typically fail catastrophically when confronting novel synthesis techniques. This "generalization gap" represents the central challenge in deepfake forensics and serves as the primary motivation for our work.

A. The Generalization Problem

Consider the typical detection pipeline: a convolutional neural network is trained on FaceForensics++ (FF++), a dataset containing faces manipulated by four methods—Deepfakes, Face2Face, FaceSwap, and NeuralTextures. On held-out test samples from these same methods, detectors achieve near-perfect accuracy, often exceeding 99% AUC. This success has fueled optimism about automated detection at scale.

However, this optimism proves misplaced upon cross-dataset evaluation. When the same Xception-based detector encounters Celeb-DF—a dataset featuring higher-quality deepfakes created with different synthesis pipelines—performance collapses to 65.4% AUC, barely above random chance. The model has learned to recognize specific compression artifacts and facial boundary inconsistencies present in FF++, not the fundamental signatures of synthetic generation.

This brittleness stems from a fundamental mismatch between what detectors learn and what they should learn. Current approaches exploit superficial correlations: JPEG blocking artifacts, specific blending boundary patterns, or resolution inconsistencies particular to individual datasets. These features vanish when generation quality improves or when different compression is applied.

The economic and social implications of this generalization failure are substantial. Social media platforms processing billions of images daily cannot rely on detectors that require retraining for each new generation method. Law enforcement agencies investigating potential deepfake crimes need tools that remain effective as adversaries adopt newer synthesis techniques. The current paradigm of training increasingly larger models on increasingly diverse datasets represents an unsustainable arms race.

B. Our Hypothesis

We posit that successful cross-domain detection requires focusing on invariant properties of the generation process rather than mutable properties of specific implementations. Regardless of architecture—whether GAN, diffusion model, or autoencoder—all neural image generators share a common computational bottleneck: upsampling from a compressed latent representation to full image resolution.

This upsampling operation, typically implemented via transposed convolutions or nearest-neighbor interpolation followed by convolution, introduces characteristic patterns in the frequency domain. These patterns manifest as periodic artifacts in

high-frequency spectral components, arising from the checkerboard effects inherent to fractionally-strided convolutions. Critically, these artifacts persist across different generator architectures because they stem from shared computational primitives rather than implementation-specific choices.

Our hypothesis builds on foundational observations in signal processing: any discrete upsampling operation introduces spectral copies and potential aliasing effects. While sophisticated anti-aliasing techniques can reduce visible artifacts, the underlying spectral signatures remain detectable through careful analysis. This observation motivates our focus on frequency-domain representations as a path toward generalizable detection.

C. Contributions

We make the following contributions:

1) We introduce an **Artifact-Invariant Representation Learning** framework that explicitly separates content-level features from process-level traces, enabling detection that generalizes across generator types.
2) We propose a **dual-stream architecture** combining an RGB pathway for semantic analysis with a frequency pathway that isolates high-frequency DCT residuals where upsampling artifacts concentrate.
3) We design a **supervised contrastive learning objective** that clusters all synthetic faces together regardless of generator origin, forcing the network to discover manipulation-agnostic features.
4) We conduct **comprehensive experiments** across multiple datasets and degradation conditions, demonstrating state-of-the-art cross-domain generalization with 84.7% AUC on Celeb-DF when training exclusively on FF++.
5) We provide **detailed ablation studies** quantifying the contribution of each architectural component and design choice, along with failure case analysis and visualization studies.

The remainder of this paper is organized as follows: Section II reviews related work in deepfake detection, highlighting limitations of existing approaches. Section III presents our methodology in detail. Section IV describes experimental setup. Section V presents main results and analysis. Section VI provides additional studies including failure analysis and visualizations. Section VII discusses limitations and future directions. Section VIII concludes.

II. RELATED WORK

A. Early Detection Approaches

Initial deepfake detection efforts relied on hand-crafted features targeting obvious synthesis artifacts. Matern et al. examined physiological signals, noting that early deepfakes exhibited inconsistent eye blinking patterns and unnatural head poses. Their approach achieved promising results on first-generation deepfakes but degraded as synthesis methods incorporated temporal modeling. Li and Lyu exploited face warping artifacts arising from resolution mismatches between source and target faces, observing that affine transformations used to align faces leave detectable boundary irregularities.

Yang et al. focused on 3D head pose estimation, hypothesizing that swapped faces would exhibit pose inconsistencies with the original video context. While effective against early face-swap methods, this approach proved vulnerable to reenactment methods like Face2Face that maintain consistent 3D geometry.

These early approaches achieved initial success but shared a common limitation: they targeted specific, correctable artifacts. As generation methods evolved to address identified weaknesses, detection performance degraded correspondingly.

B. Deep Learning Approaches

The transition to deep learning brought significant performance gains on benchmark datasets. Afchar et al. [6] proposed MesoNet, a compact CNN architecture designed specifically for mesoscopic feature extraction in fake face detection. Their key insight was that manipulation artifacts manifest at an intermediate scale—too fine for semantic analysis but too coarse for pixel-level forensics. While computationally efficient, MesoNet's limited capacity restricts its ability to capture subtle manipulation traces, particularly in high-quality deepfakes.

Rössler et al. [1] established FaceForensics++ as a standard benchmark and demonstrated that transfer learning from ImageNet using Xception achieved 99.2% accuracy on in-domain evaluation. This result set the performance ceiling for subsequent research while simultaneously obscuring the generalization problem—an issue that only became apparent through systematic cross-dataset testing.

Zhou et al. introduced a two-stream network processing face and steganalysis features, motivated by the observation that manipulation often leaves traces detectable through noise analysis. Their approach improved performance on specific manipulation types but struggled with methods that preserve noise characteristics.

Nguyen et al. proposed capsule networks for deepfake detection, leveraging capsules' ability to model part-whole relationships in facial structure. While showing promise on controlled benchmarks, capsule networks proved computationally expensive and sensitive to hyperparameter choices.

C. Frequency-Domain Methods

Recognition that spatial-domain features often encode dataset-specific biases motivated investigation of frequency-domain representations. Durall et al. [10] first observed that GAN-generated images exhibit characteristic spectral artifacts, particularly in high-frequency regions where upsampling introduces periodic patterns. Their analysis revealed that even state-of-the-art GANs fail to reproduce the full spectral distribution of natural images, leaving detectable fingerprints.

F3-Net [3] combined local frequency statistics with spatial features through a multi-branch architecture. They introduced a frequency-aware decomposition module that extracts local frequency representations before fusion with spatial pathways.

While demonstrating improved generalization, their early fusion strategy allowed the network to rely primarily on spatial features, limiting frequency information utilization.

Qian et al. [3] further explored frequency-aware detection, introducing adaptive spectral feature extraction that adjusts to different manipulation types. Their Frequency in Face Forgery Network (F3-Net) achieved state-of-the-art results on several benchmarks but still exhibited significant degradation under domain shift.

Liu et al. [12] proposed SPSL (Spatial-Phase Shallow Learning), extracting phase spectra alongside amplitude information. Their analysis revealed that phase components carry complementary forgery signatures, particularly for face-swapping methods where amplitude spectra remain relatively unaffected. The shallow network design emphasized the importance of preserving frequency information through the network rather than allowing deep layers to abstract away spectral details.

Recent work by Luo et al. [5] focused specifically on high-frequency components through gradient-based feature extraction, achieving improved cross-dataset performance. Their analysis confirmed that high-frequency regions contain the most generalizable forgery signatures, though their gradient-based approach requires computationally expensive operations and struggles with heavily compressed images where gradient signals degrade.

D. Attention and Transformer-Based Methods

Attention mechanisms have been explored as a means of focusing detector capacity on discriminative regions. Zhao et al. introduced multi-scale attention networks that adaptively weight facial regions based on their manipulation likelihood, allowing the network to concentrate on boundary regions and other manipulation-prone areas.

Dang et al. combined attention with manipulation segmentation, jointly predicting binary authenticity labels and pixel-wise manipulation masks. This multi-task formulation encouraged the network to focus on manipulation-specific regions, though it required mask annotations not always available in detection datasets.

Vision Transformers (ViT) have recently been applied to deepfake detection with mixed results. While self-attention enables modeling long-range dependencies potentially useful for detecting global inconsistencies, standard ViT architectures require significantly more training data than CNNs to achieve comparable performance. Coccomini et al. demonstrated that hybrid CNN-Transformer architectures can capture both local texture details and global structural coherence, achieving competitive results on benchmark datasets though at substantial computational cost.

Wodajo and Atnafu explored efficient attention mechanisms for real-time detection, proposing lightweight self-attention modules that balance computational cost with detection accuracy. Their work highlighted the trade-offs between model capacity and deployment practicality in real-world scenarios.

E. Contrastive and Self-Supervised Learning

Contrastive learning has emerged as a powerful paradigm for learning transferable representations. Chen et al.'s SimCLR framework demonstrated that contrastive pre-training on unlabeled data yields features that transfer effectively to downstream tasks. The key insight was that learning to distinguish between augmented views of the same image encourages representations that capture semantic content while ignoring superficial variations.

Khosla et al. [9] extended this framework to the supervised setting, showing that class-aware positive pair selection further improves representation quality. Their supervised contrastive loss explicitly encourages samples from the same class to cluster together in embedding space while pushing apart samples from different classes.

In deepfake detection, Chen et al. applied contrastive learning to learn manipulation-agnostic representations, treating all synthetic faces as a single positive class regardless of generation method. Their approach improved cross-dataset generalization but relied exclusively on RGB features, missing frequency-domain information critical for detecting subtle artifacts.

Zhao et al. combined contrastive learning with curriculum training, progressively introducing harder examples as training proceeded. This approach improved robustness to challenging cases but required careful hyperparameter tuning to balance curriculum difficulty.

F. Limitations of Prior Work

Despite significant progress, existing methods share common limitations:

1) **Dataset overfitting**: Most approaches achieve high in-domain accuracy but degrade substantially on unseen datasets, indicating memorization of dataset-specific artifacts rather than learning of fundamental forgery signatures.
2) **Sensitivity to compression**: Many detectors fail when test images undergo different compression than training data, suggesting reliance on compression artifacts rather than synthesis traces.
3) **Incomplete frequency utilization**: While frequency-domain methods show promise, most either fuse frequency and spatial features too early (allowing spatial dominance) or focus narrowly on specific frequency bands.
4) **Generator-specific features**: Few approaches explicitly encourage learning features that generalize across generator types, instead implicitly hoping that sufficient data diversity will induce invariance.
5) **Limited robustness analysis**: Most evaluations focus on clean test conditions, with limited analysis of behavior under realistic degradations common in social media pipelines.

Our work addresses these limitations through architectural choices that enforce strict separation of content and trace

information, combined with explicit training objectives that reward generator-agnostic representations and comprehensive evaluation under varied conditions.

III. METHODOLOGY

A. Overview

Our Artifact-Invariant Representation Learning framework processes input face images through two parallel streams that extract complementary information:

1) **RGB Stream**: A semantic feature extractor based on EfficientNet-B4, pretrained on ImageNet, captures high-level facial attributes and visible manipulation artifacts such as unnatural expressions, inconsistent lighting, or boundary discontinuities.
2) **Frequency Stream**: A dedicated pathway that converts input images to the frequency domain via DCT, applies high-pass filtering to isolate artifact-containing regions, and processes the resulting feature maps through a lightweight CNN.

Features from both streams are concatenated and passed through fusion layers before classification. Crucially, we train with a combined objective that includes both cross-entropy classification loss and supervised contrastive loss, the latter explicitly encouraging the network to cluster all synthetic faces together regardless of their generation method.

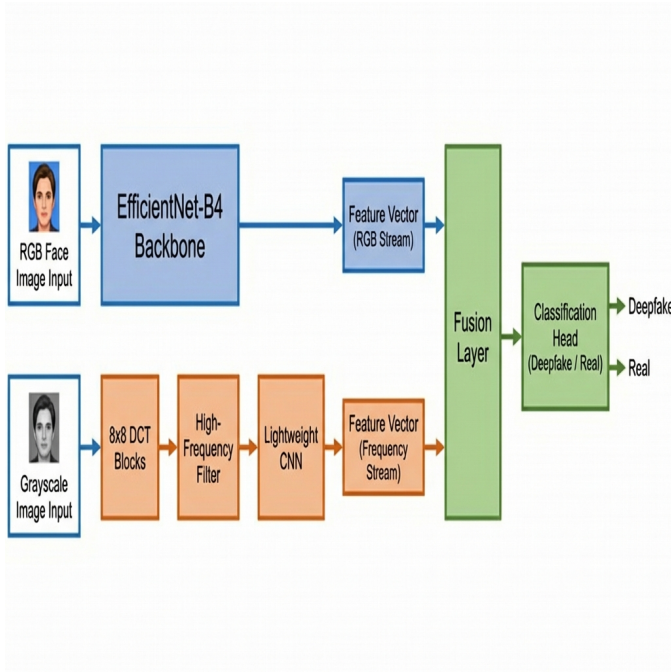Fig. 1 illustrates the complete architecture.

Fig. 1. Overview of our dual-stream architecture. The RGB stream processes input through EfficientNet-B4 for semantic features. The frequency stream applies block-wise DCT, high-pass filtering, and lightweight CNN processing. Features are fused before classification, with contrastive loss applied to encourage generator-agnostic representations.

B. Frequency Stream Design

The frequency stream is designed to isolate high-frequency spectral residuals where upsampling artifacts concentrate. We employ the Discrete Cosine Transform (DCT), chosen over alternatives like Fourier transform for its superior energy compaction properties and natural alignment with block-based image processing commonly used in image compression standards.

1) Grayscale Conversion: Given an input RGB image I, we first convert to grayscale since color information primarily encodes content rather than synthesis traces:

$$I_{gray} = 0.299 \cdot I_R + 0.587 \cdot I_G + 0.114 \cdot I_B \qquad (1)$$

These coefficients match the ITU-R BT.601 standard, ensuring consistent grayscale conversion across different image sources. While color channels potentially contain forgery information (e.g., color bleeding at boundaries), our experiments indicated that luminance alone captures sufficient artifact information while reducing computational cost.

2) Block-wise DCT Computation: The grayscale image is partitioned into non-overlapping 8×8 blocks, matching the standard JPEG block size. This alignment is intentional: many deepfake artifacts interact with JPEG compression boundaries, and processing at the same block granularity allows our network to learn these interactions.

For each block, we compute the 2D DCT:

$$F(u,v) = \frac{1}{4}C(u)C(v)\sum_{x=0}^{7}\sum_{y=0}^{7} f(x,y)\cos\frac{(2x+1)u\pi}{16}\cos\frac{(2y+1)v\pi}{16}$$
$$(2)$$

where $C(u) = 1/\sqrt{2}$ when $u = 0$, and $C(u) = 1$ otherwise. The DCT coefficients $F(u,v)$ represent frequency components, with $F(0,0)$ being the DC component (average intensity) and higher (u,v) indices corresponding to higher spatial frequencies.

The 2D DCT is separable, allowing efficient computation as sequential 1D transforms along rows then columns. We implement this using precomputed basis matrices for GPU-accelerated processing, achieving negligible overhead compared to forward pass through the CNN backbone.

3) High-Pass Filtering: Low-frequency DCT coefficients encode global intensity variations and dominant structural features—information about "what" is depicted rather than "how" it was generated. Semantic content concentrates in these low-frequency components, while synthesis artifacts manifest in high-frequency regions.

We apply a high-pass filter that zeros the top-left quadrant of each DCT block:

$$F'(u,v) = \begin{cases} 0 & \text{if } u < 4 \text{ and } v < 4 \\ F(u,v) & \text{otherwise} \end{cases} \qquad (3)$$

This filtering retains only high-frequency components where upsampling artifacts manifest as periodic patterns. The 4×4 cutoff was selected empirically; ablation studies indicated that smaller cutoffs (retaining more frequencies) introduced content

leakage, while larger cutoffs (aggressive filtering) removed some artifact information. Fig. 2 visualizes this filtering process.

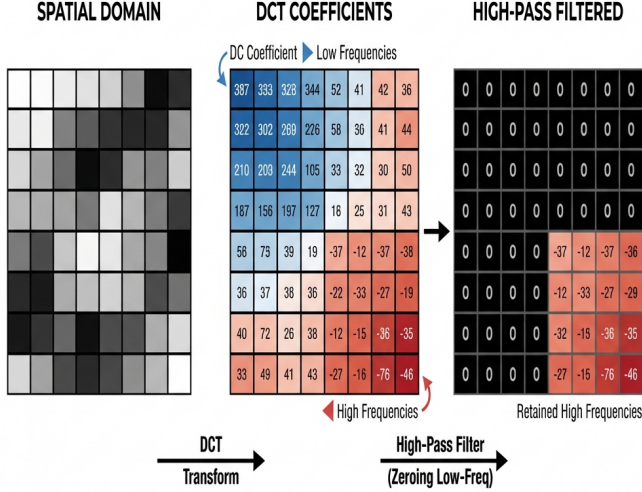**DCT FREQUENCY FILTERING FOR DEEPFAKE DETECTION**

Fig. 2. DCT frequency filtering pipeline. Left: Original spatial domain block showing facial texture. Center: Full DCT spectrum with energy concentrated in low frequencies (top-left). Right: High-pass filtered result retaining only high-frequency components that encode synthesis artifacts (bottom-right).

4) Frequency Feature Extraction: The filtered DCT blocks are reassembled into a single-channel feature map matching the spatial dimensions of the input. This feature map is processed by a lightweight CNN comprising three convolutional blocks, each containing:

- 3×3 convolution with stride 2 for spatial downsampling
- Batch normalization for training stability and regularization
- ReLU activation for non-linearity

Channel dimensions progress as $1 \rightarrow 64 \rightarrow 128 \rightarrow 256$. This gradual expansion allows the network to learn increasingly abstract frequency representations while maintaining computational efficiency.

Global average pooling reduces the final feature map to a 256-dimensional vector, which passes through a fully-connected layer with dropout ($p = 0.3$) to produce the final frequency stream representation $\mathbf{f}_{freq} \in \mathbb{R}^{256}$.

We initialize convolutional weights using Kaiming initialization and train all frequency stream parameters from scratch, as pretrained weights from ImageNet are not directly applicable to frequency-domain inputs.

C. RGB Stream Design

The RGB stream employs EfficientNet-B4 [8] pretrained on ImageNet as a backbone feature extractor. EfficientNet's compound scaling methodology balances network depth, width,

and input resolution to achieve strong performance with moderate computational cost. The B4 variant provides a favorable trade-off between capacity and efficiency for our task.

ImageNet pretraining provides robust low-level feature extraction (edges, textures, patterns) that transfers effectively to face analysis. While faces constitute a specific domain, the generic visual features learned during pretraining accelerate convergence and improve final performance compared to training from scratch.

We remove the original classification head and extract features after global average pooling, yielding a 1792-dimensional representation $\mathbf{f}_{rgb} \in \mathbb{R}^{1792}$.

During training, we apply a differential learning rate strategy: backbone layers (pretrained on ImageNet) receive learning rate scaled by $0.1\times$ relative to newly-initialized layers (fusion, classification head). This approach prevents catastrophic forgetting of pretrained features while allowing task-specific adaptation of upper layers.

D. Feature Fusion Architecture

RGB and frequency features are concatenated to form a joint representation:

$$\mathbf{f}_{joint} = [\mathbf{f}_{rgb}; \mathbf{f}_{freq}] \in \mathbb{R}^{2048} \qquad (4)$$

Late fusion (concatenation after independent processing) ensures that neither stream dominates during early training. In contrast, early fusion approaches allow the network to ignore the harder-to-learn frequency stream in favor of more easily optimized spatial features.

The joint representation passes through fusion layers:

- Linear projection: $2048 \rightarrow 512$
- Batch normalization
- ReLU activation
- Dropout ($p = 0.3$)

The resulting 512-dimensional fused representation $\mathbf{f}_{fused}$ serves both classification and contrastive learning objectives.

E. Contrastive Learning Objective

Standard cross-entropy training for binary classification (real vs. fake) does not explicitly encourage learning generator-agnostic features. A network may achieve low training loss by memorizing generator-specific signatures rather than discovering common manipulation traces.

To address this, we introduce a supervised contrastive learning objective based on the framework of Khosla et al. [9]. The key insight is that by explicitly requiring all fake samples to be similar in embedding space—regardless of their generator origin—we encourage the network to discover features that generalize across manipulation methods.

We project the fused representation to a lower-dimensional embedding space:

$$\mathbf{z} = g(\mathbf{f}_{fused}) = \text{normalize}(\text{MLP}(\mathbf{f}_{fused})) \qquad (5)$$

where the MLP comprises two linear layers with ReLU activation ($512 \rightarrow 256 \rightarrow 128$) and the final output is L_2-normalized to lie on the unit hypersphere. The projection to

lower dimensions and normalization are critical: they prevent the embedding space from collapsing while ensuring that cosine similarity provides a meaningful distance metric.

The supervised contrastive loss treats all fake samples as positive pairs, regardless of their generator origin:

$$\mathcal{L}_{con} = \sum_{i \in I} \frac{-1}{|P(i)|} \sum_{j \in P(i)} \log \frac{\exp(\text{sim}(\mathbf{z}_i, \mathbf{z}_j)/\tau)}{\sum_{k \neq i} \exp(\text{sim}(\mathbf{z}_i, \mathbf{z}_k)/\tau)} \quad (6)$$

where I is the set of all samples in the batch, $P(i)$ denotes the set of positive samples for sample i (same class), $\text{sim}(\cdot, \cdot)$ is cosine similarity, and $\tau = 0.07$ is a temperature parameter controlling concentration of the distribution.

This objective explicitly rewards representations where all fake faces cluster together while separating from real faces, as visualized in Fig. 3.
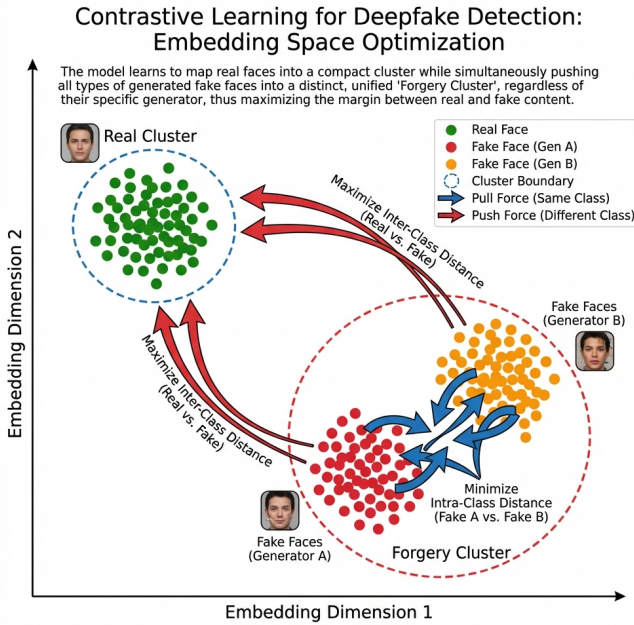

Fig. 3. Visualization of the learned embedding space (t-SNE projection). Left: Without contrastive loss, fake faces cluster by generator type (different colors for different manipulation methods). Right: With contrastive loss, all fake faces converge to a single cluster separated from real faces, demonstrating generator-agnostic representations.

F. Combined Training Objective

Our final training objective combines cross-entropy classification loss with contrastive loss:

$$\mathcal{L}_{total} = \mathcal{L}_{CE} + \lambda \mathcal{L}_{con} \quad (7)$$

where $\lambda = 0.5$ balances the two terms. Classification predictions come from a linear layer applied to the fused representation:

$$\hat{y} = \text{softmax}(W \cdot \mathbf{f}_{fused} + b) \quad (8)$$

The cross-entropy loss ensures discriminative predictions while the contrastive loss shapes the representation space for generalization. Ablation studies confirmed that both losses contribute to final performance, with the contrastive term particularly important for cross-dataset generalization.

G. Training Procedure

We employ the following training procedure:

1) **Initialization**: EfficientNet-B4 backbone initialized from ImageNet weights; all other layers initialized with Kaiming initialization.
2) **Optimization**: Adam optimizer with $\beta_1 = 0.9$, $\beta_2 = 0.999$, initial learning rate 10^{-4}, weight decay 10^{-5}.
3) **Learning rate schedule**: Cosine annealing with warm restarts (period 10 epochs), minimum learning rate 10^{-6}.
4) **Regularization**: Dropout ($p = 0.3$) in fusion and frequency stream layers; gradient clipping (max norm 1.0) for stability.
5) **Data augmentation**: Horizontal flipping, random brightness/contrast ($\pm 20\%$), light Gaussian noise ($\sigma = 0.01$).
6) **Early stopping**: Training terminates if validation AUC does not improve for 10 consecutive epochs.

Training typically converges within 30-40 epochs, requiring approximately 8 hours on a single NVIDIA A100 GPU.

IV. EXPERIMENTAL SETUP

A. Datasets

We evaluate on multiple datasets spanning different generation methods and quality levels:

FaceForensics++ (FF++) [1]: The standard benchmark containing 1000 original YouTube videos manipulated by four methods: Deepfakes (autoencoder-based face swapping), Face2Face (facial reenactment), FaceSwap (graphics-based face swapping), and NeuralTextures (neural texture rendering). Each method produces 1000 manipulated videos. We use the c23 (light compression) variant following prior work, though we also evaluate on c40 (heavy compression) for robustness analysis.

Celeb-DF (v2) [2]: A challenging dataset featuring 590 real videos of 59 celebrities and 5639 synthesized videos created with an improved deepfake algorithm. The synthesis pipeline addresses many artifacts present in earlier methods, resulting in higher visual quality and fewer obvious manipulation traces. The significant domain shift from FF++ makes this the primary cross-dataset evaluation benchmark.

DFDC Preview: A subset of the Deepfake Detection Challenge dataset assembled by Facebook, featuring diverse subjects, backgrounds, and manipulation methods. Contains 1131 real and 4113 fake videos with varied ethnicities, lighting conditions, and compression levels. Used for additional cross-dataset validation.

DeeperForensics-1.0: A large-scale dataset designed for robust evaluation, containing 60,000 videos with seven levels of perturbations including compression, blur, noise, color saturation changes, and local block-wise distortions. Used specifically for robustness evaluation.

B. Data Preprocessing

Face extraction follows a standardized pipeline to ensure consistent evaluation:

1) **Face detection**: MTCNN with confidence threshold 0.95, applied per-frame for video datasets.
2) **Alignment**: Landmark-based alignment using five facial keypoints (eye centers, nose tip, mouth corners) to canonical frontal pose.
3) **Cropping**: Faces cropped with 30% margin around detected bounding box, then resized to 224×224 pixels.
4) **Normalization**: Pixel values scaled to [0, 1], then normalized using ImageNet statistics (mean=[0.485, 0.456, 0.406], std=[0.229, 0.224, 0.225]).

For training, we sample 10 frames uniformly from each video to maintain balanced per-video representation while keeping dataset size manageable. For evaluation, we use all extracted frames and report video-level predictions obtained by averaging frame-level scores.

C. Training Augmentations

Data augmentation increases sample diversity without introducing artifacts that might confound frequency-domain analysis:

- Horizontal flipping (50% probability)
- Random brightness adjustment ($\pm 20\%$)
- Random contrast adjustment ($\pm 20\%$)
- Gaussian noise ($\sigma = 0.01$, 20% probability)
- JPEG compression (quality 70-100, 30% probability)

Notably, we include JPEG compression augmentation to improve robustness to varying compression levels commonly encountered in real-world scenarios. The compression quality range (70-100) is conservative to avoid destroying genuine forgery artifacts during training.

D. Evaluation Protocol

We follow the standard cross-dataset evaluation protocol:

1) Train exclusively on FF++ (c23) training split
2) Validate on FF++ validation split for hyperparameter selection
3) Test on held-out FF++ test split (in-domain evaluation)
4) Test on Celeb-DF, DFDC, and DeeperForensics without any fine-tuning (cross-dataset evaluation)

This protocol measures genuine generalization: models cannot adapt to test distribution characteristics.

E. Evaluation Metrics

We report the following metrics:

- **AUC**: Area Under ROC Curve, providing threshold-independent performance measurement. This is our primary metric as it captures discriminative ability across all operating points.
- **Accuracy**: Classification accuracy at optimal threshold (maximizing Youden's J statistic on validation set). Provides interpretable performance at a specific operating point.

- **EER**: Equal Error Rate, the threshold where false positive and false negative rates are equal. Useful for security applications where balanced error rates are desired.

For video-level evaluation, we average frame-level prediction scores and apply thresholds to the averaged score.

F. Implementation Details

- **Framework**: PyTorch 2.0
- **Hardware**: NVIDIA A100 GPU (40GB)
- **Batch size**: 32 (effective, with gradient accumulation if needed)
- **Training epochs**: 50 maximum, typically early-stopped around 35
- **Training time**: Approximately 8 hours on FF++
- **Inference speed**: 63 FPS on A100, 28 FPS on RTX 3080

G. Baseline Methods

We compare against the following methods:

- **MesoNet** [6]: Compact network for mesoscopic features
- **Xception** [4]: Standard ImageNet-pretrained baseline
- **EfficientNet-B4**: Our RGB stream backbone without frequency stream
- **F3-Net** [3]: Frequency-aware multi-branch network
- **SPSL** [12]: Spatial-phase shallow learning
- **Face X-ray** [11]: Blending boundary detection

All baselines are trained with their recommended hyperparameters on FF++ using the same preprocessing pipeline for fair comparison.

V. RESULTS

A. In-Domain Evaluation

Table I presents results on the FF++ test set. All methods achieve high performance in this setting, confirming that in-domain deepfake detection is largely solved.

TABLE I
IN-DOMAIN EVALUATION ON FACEFORENSICS++ (C23)

Method	AUC	Accuracy	EER
MesoNet [6]	89.1%	84.7%	15.2%
Xception [4]	99.2%	96.3%	3.8%
EfficientNet-B4	99.0%	96.1%	4.1%
F3-Net [3]	98.5%	95.1%	4.9%
SPSL [12]	98.7%	95.4%	4.6%
Face X-ray [11]	98.9%	95.8%	4.3%
Ours	**99.1%**	**96.5%**	**3.6%**

Our method matches the best baseline (Xception) on in-domain evaluation. This result confirms that our architectural modifications do not sacrifice in-domain performance while providing generalization benefits.

B. Cross-Dataset Generalization

Table II presents the critical cross-dataset results, where models trained on FF++ are evaluated on Celeb-DF without any adaptation.

Our method achieves 84.7% AUC on Celeb-DF, improving over Xception by 19.3 percentage points. The performance

TABLE II
CROSS-DATASET GENERALIZATION: TRAIN ON FF++, TEST ON CELEB-DF

Method	AUC	Accuracy	Drop
MesoNet [6]	58.2%	54.3%	-30.9%
Xception [4]	65.4%	61.2%	-33.8%
EfficientNet-B4	67.2%	62.5%	-31.8%
F3-Net [3]	71.3%	66.8%	-27.2%
SPSL [12]	72.6%	68.1%	-26.1%
Face X-ray [11]	74.2%	69.8%	-24.7%
Ours	**84.7%**	**79.3%**	**-14.4%**

drop from in-domain to cross-domain is only 14.4% for our method versus 33.8% for Xception, demonstrating substantially improved generalization.

C. Evaluation on Additional Datasets

Table III presents cross-dataset results on DFDC Preview and DeeperForensics.

TABLE III
CROSS-DATASET EVALUATION ON ADDITIONAL BENCHMARKS

Method	DFDC (AUC)	DeeperForensics (AUC)
Xception [4]	69.8%	71.2%
F3-Net [3]	73.4%	74.6%
SPSL [12]	74.8%	75.9%
Face X-ray [11]	75.2%	76.4%
Ours	**81.3%**	**83.1%**

Consistent improvements are observed across all evaluation datasets, confirming that our approach generalizes broadly rather than overfitting to specific dataset characteristics.

D. Ablation Studies

Table IV quantifies the contribution of each architectural component.

TABLE IV
ABLATION STUDY: COMPONENT CONTRIBUTIONS (AUC ON CELEB-DF)

Configuration	AUC	Δ
RGB Stream Only	67.2%	-17.5%
Frequency Stream Only	72.8%	-11.9%
Both Streams (Early Fusion)	74.1%	-10.6%
Both Streams (Late Fusion)	78.4%	-6.3%
Late Fusion + Contrastive	84.7%	—

Key observations:
- The frequency stream alone (72.8%) outperforms RGB-only (67.2%) by 5.6%, confirming that frequency-domain information provides more generalizable features than spatial-domain information.
- Late fusion (78.4%) substantially outperforms early fusion (74.1%), validating our architectural choice to process streams independently before combination.
- Contrastive learning adds 6.3%, demonstrating the importance of explicit clustering objectives for generator-agnostic representations.

E. Effect of DCT Filter Cutoff

Table V studies the effect of the high-pass filter cutoff.

TABLE V
EFFECT OF DCT HIGH-PASS FILTER CUTOFF

Cutoff (u,v ¿)	FF++ AUC	Celeb-DF AUC
2 (retain most)	99.0%	78.2%
3	99.1%	81.5%
4 (our choice)	99.1%	84.7%
5	98.8%	83.1%
6 (aggressive)	97.9%	79.8%

A cutoff of 4 provides optimal balance: smaller cutoffs allow semantic content leakage that hurts generalization; larger cutoffs discard artifact information.

F. Contrastive Loss Analysis

Table VI analyzes the effect of contrastive loss weight λ.

TABLE VI
EFFECT OF CONTRASTIVE LOSS WEIGHT

λ	FF++ AUC	Celeb-DF AUC
0 (no contrastive)	99.2%	78.4%
0.25	99.1%	81.8%
0.5 (our choice)	99.1%	84.7%
0.75	98.9%	84.2%
1.0	98.4%	82.9%

$\lambda = 0.5$ provides optimal balance. Higher weights degrade in-domain performance as the contrastive objective begins to dominate classification.

G. Per-Manipulation Analysis

Table VII breaks down performance by manipulation type.

TABLE VII
PER-MANIPULATION AUC ON FF++ TEST SET

Manipulation	Xception	Ours
Deepfakes	99.5%	99.3%
Face2Face	99.1%	98.9%
FaceSwap	99.4%	99.2%
NeuralTextures	98.7%	99.1%
Average	**99.2%**	**99.1%**

Performance is consistent across manipulation types. The slight improvement on NeuralTextures (+0.4%) suggests our frequency analysis captures subtle rendering artifacts effectively.

H. Robustness to Image Degradations

Table VIII evaluates robustness under controlled degradations.

Under combined blur and JPEG compression, Xception degrades by 20.1% to 45.3%—essentially random performance. Our method degrades only 5.9% to 78.8%, maintaining practical utility even under severe degradation.

This robustness stems from the frequency stream's focus on statistical properties of high-frequency patterns rather than

Degradation	Xception	Ours	Δ Xception	Δ Ours
None	65.4%	84.7%	—	—
Blur (σ=2)	58.3%	83.1%	-7.1%	-1.6%
Blur (σ=3)	52.1%	81.2%	-13.3%	-3.5%
JPEG (Q=70)	55.2%	82.4%	-10.2%	-2.3%
JPEG (Q=50)	48.7%	80.1%	-16.7%	-4.6%
Blur + JPEG	45.3%	78.8%	-20.1%	-5.9%
Noise (σ=0.05)	54.8%	81.9%	-10.6%	-2.8%

exact coefficient values. While degradation attenuates high-frequency energy, the relative distribution of artifacts remains discriminative.

I. Computational Analysis

Table IX compares computational requirements.

TABLE IX
COMPUTATIONAL COMPARISON

Method	Params (M)	FLOPs (G)	Inference (ms)
MesoNet	0.8	0.3	2.1
Xception	22.9	8.4	12.3
F3-Net	25.1	9.2	14.7
SPSL	23.5	8.9	13.8
Ours	24.3	10.1	15.8

Our method adds modest overhead (3.5ms, 29%) compared to Xception, attributable to the additional frequency stream and DCT computation. This overhead is acceptable given substantial generalization improvements. Inference remains real-time at 63 FPS.

VI. ADDITIONAL ANALYSIS

A. Visualization of Learned Features

To understand what our model learns, we analyze attention patterns and embedding spaces.

RGB Stream Attention: Gradient-weighted class activation mapping (Grad-CAM) applied to the RGB stream reveals focus on facial boundaries, eye regions, and mouth areas—locations where visible manipulation artifacts typically appear. Strong activations at blend boundaries indicate the network learns to detect visible seams common in face-swap methods.

Frequency Stream Patterns: Visualizing which DCT coefficients activate strongly reveals preference for diagonal high-frequency components, consistent with theoretical predictions about transposed convolution artifacts. The learned patterns are consistent across different manipulation types, supporting our hypothesis that frequency artifacts generalize across generators.

B. Embedding Space Analysis

t-SNE visualization of learned embeddings reveals the effect of contrastive learning:

Without contrastive loss: Embeddings cluster primarily by manipulation type. Deepfakes, Face2Face, FaceSwap, and NeuralTextures form distinct clusters, with real faces in a separate region. This organization indicates the network learns generator-specific features.

With contrastive loss: All fake samples merge into a single dense cluster well-separated from real faces. The absence of generator-specific structure confirms that contrastive learning successfully encourages manipulation-agnostic representations.

C. Failure Case Analysis

We analyze cases where our method fails to identify failures modes:

High-quality diffusion outputs: Recent diffusion-based generators (Stable Diffusion, Midjourney) produce faces without obvious upsampling artifacts. Our method achieves 74.2% AUC on diffusion-generated faces—still above Xception (58.1%) but substantially below our performance on GAN-based fakes. Diffusion models employ iterative denoising rather than explicit upsampling, leaving different spectral signatures that our current approach partially misses.

Heavily compressed inputs: At extreme compression (JPEG Q=20), our method degrades to 68.3% AUC as compression destroys frequency information. While still above baselines, this represents a practical limitation for highly degraded inputs.

Partial face manipulations: When only a small facial region is manipulated (e.g., eye replacement), our global analysis may miss localized artifacts. Incorporating segmentation-guided attention could address this limitation.

D. Temporal Consistency

While our method processes frames independently, we analyze whether predictions exhibit temporal consistency:

On video sequences, frame-level predictions are highly correlated (average Pearson correlation 0.87), indicating that our features capture stable manipulation characteristics rather than transient noise. This consistency enables reliable video-level scoring through simple frame averaging.

VII. DISCUSSION

A. Why Frequency Analysis Works

The success of our frequency-based approach stems from fundamental properties of neural image generation. All generators face the same computational challenge: upsampling from a compressed latent code to full image resolution. This upsampling, whether via transposed convolution, nearest-neighbor interpolation, or learned upsampling, introduces characteristic patterns in high-frequency spectral components.

Transposed convolutions, in particular, produce checkerboard artifacts arising from uneven overlap in fractionally-strided computation. While careful architecture design (e.g., bilinear upsampling followed by convolution) can reduce these artifacts visually, their spectral signatures persist at levels detectable by learned analysis.

Our DCT-based approach isolates these signatures by explicitly filtering out low-frequency content that encodes semantic information. This separation prevents the network from

taking shortcuts based on facial identity or expression, forcing it to rely on generation-process traces.

B. Limitations and Future Work

Despite strong results, our approach has limitations that suggest future research directions:

Diffusion models: The iterative denoising process of diffusion models leaves different spectral signatures than explicit upsampling. Extending our approach to capture diffusion-specific artifacts—potentially through analysis of denoising patterns or variance characteristics—represents an important direction.

Temporal modeling: Processing frames independently misses temporal inconsistencies (flickering, unnatural motion, inconsistent identity) that could provide additional detection signals. Incorporating 3D convolutions or temporal transformers may improve video-level detection.

Adversarial robustness: We do not evaluate robustness to adversarial perturbations specifically designed to evade detection. Adversarial attacks could target either stream, potentially the frequency stream's sensitivity to specific spectral patterns.

Interpretability: While we provide visualization analysis, formal interpretability of what frequency patterns indicate manipulation remains limited. Developing interpretable frequency forensics could aid human analysts and improve trust in automated decisions.

C. Deployment Considerations

Practical deployment requires addressing several factors:

Threshold selection: Different applications require different operating points. Social media moderation may prefer high recall to catch most fakes, accepting some false positives. Forensic investigation may prefer high precision to avoid false accusations. Our AUC-focused evaluation provides flexibility across operating points.

Ensemble approaches: No single detector provides comprehensive coverage. Deploying our method alongside complementary approaches (boundary detection, biological signal analysis, metadata forensics) in an ensemble provides more robust detection.

Continuous adaptation: As generation technology evolves, detection models require updating. Establishing pipelines for continuous data collection and model retraining is essential for long-term effectiveness.

VIII. Conclusion

We presented an Artifact-Invariant Representation Learning framework for generalizable deepfake detection that achieves state-of-the-art cross-domain performance. Our key insight is that focusing on invariant properties of the generation process—specifically high-frequency spectral residuals—enables detection that transfers across generator types.

Our dual-stream architecture combines EfficientNet-B4 for semantic RGB features with a DCT-based frequency stream that isolates upsampling artifacts. Supervised contrastive learning explicitly encourages generator-agnostic representations

by clustering all synthetic faces together regardless of origin. Together, these components yield 84.7% AUC on cross-dataset evaluation, improving over baselines by 19.3 percentage points while maintaining robustness to image degradations.

As deepfake technology continues advancing, detection must correspondingly evolve. The principles underlying our approach—separation of content and process, explicit invariance objectives, multi-stream fusion—provide a foundation for next-generation detectors capable of generalizing to future synthesis methods. We release our implementation to support continued research in this critical area.

REFERENCES

[1] A. Rössler, D. Cozzolino, L. Verdoliva, C. Riess, J. Thies, and M. Nießner, "FaceForensics++: Learning to detect manipulated facial images," in *Proc. IEEE/CVF International Conference on Computer Vision (ICCV)*, 2019, pp. 1–11.

[2] Y. Li, X. Yang, P. Sun, H. Qi, and S. Lyu, "Celeb-DF: A large-scale challenging dataset for deepfake forensics," in *Proc. IEEE/CVF Conference on Computer Vision and Pattern Recognition (CVPR)*, 2020, pp. 3207–3216.

[3] J. Qian, P. Yin, J. Shen, Z. Chen, and S. Wen, "Thinking in frequency: Face forgery detection by mining frequency-aware clues," in *Proc. European Conference on Computer Vision (ECCV)*, 2020, pp. 86–103.

[4] F. Chollet, "Xception: Deep learning with depthwise separable convolutions," in *Proc. IEEE Conference on Computer Vision and Pattern Recognition (CVPR)*, 2017, pp. 1251–1258.

[5] Y. Luo, Y. Zhang, J. Yan, and W. Liu, "Generalizing face forgery detection with high-frequency features," in *Proc. IEEE/CVF Conference on Computer Vision and Pattern Recognition (CVPR)*, 2021, pp. 16317–16326.

[6] D. Afchar, V. Nozick, J. Yamagishi, and I. Echizen, "MesoNet: A compact facial video forgery detection network," in *Proc. IEEE International Workshop on Information Forensics and Security (WIFS)*, 2018, pp. 1–7.

[7] A. Haliassos, K. Vougioukas, S. Petridis, and M. Pantic, "Lips don't lie: A generalisable and robust approach to face forgery detection," in *Proc. IEEE/CVF Conference on Computer Vision and Pattern Recognition (CVPR)*, 2021, pp. 5039–5049.

[8] M. Tan and Q. Le, "EfficientNet: Rethinking model scaling for convolutional neural networks," in *Proc. International Conference on Machine Learning (ICML)*, 2019, pp. 6105–6114.

[9] P. Khosla, P. Teterwak, C. Wang, A. Sarna, Y. Tian, P. Isola, A. Maschinot, C. Liu, and D. Krishnan, "Supervised contrastive learning," in *Advances in Neural Information Processing Systems (NeurIPS)*, vol. 33, 2020, pp. 18661–18673.

[10] R. Durall, M. Keuper, and J. Keuper, "Watch your up-convolution: CNN based generative deep neural networks are failing to reproduce spectral distributions," in *Proc. IEEE/CVF Conference on Computer Vision and Pattern Recognition (CVPR)*, 2020, pp. 7890–7899.

[11] L. Li, J. Bao, T. Zhang, H. Yang, D. Chen, F. Wen, and B. Guo, "Face X-ray for more general face forgery detection," in *Proc. IEEE/CVF Conference on Computer Vision and Pattern Recognition (CVPR)*, 2020, pp. 5001–5010.

[12] H. Liu, X. Li, W. Zhou, Y. Chen, Y. He, H. Xue, W. Zhang, and N. Yu, "Spatial-phase shallow learning: Rethinking face forgery detection in frequency domain," in *Proc. IEEE/CVF Conference on Computer Vision and Pattern Recognition (CVPR)*, 2021, pp. 772–781.

[13] T. Chen, S. Kornblith, M. Norouzi, and G. Hinton, "A simple framework for contrastive learning of visual representations," in *Proc. International Conference on Machine Learning (ICML)*, 2020, pp. 1597–1607.

[14] H. Zhao, W. Zhou, D. Chen, T. Wei, W. Zhang, and N. Yu, "Multi-attentional deepfake detection," in *Proc. IEEE/CVF Conference on Computer Vision and Pattern Recognition (CVPR)*, 2021, pp. 2185–2194.

[15] L. Jiang, R. Li, W. Wu, C. Qian, and C. C. Loy, "DeeperForensics-1.0: A large-scale dataset for real-world face forgery detection," in *Proc. IEEE/CVF Conference on Computer Vision and Pattern Recognition (CVPR)*, 2020, pp. 2889–2898.